ACS Biomaterials SCIENCE & ENGINEERING

Article

Cite This: ACS Biomater. Sci. Eng. 2018, 4, 3347−3355

pubs.acs.org/journal/abseba

Modulating Bone Regeneration in Rabbit Condyle Defects with Three Surface-Structured Tricalcium Phosphate Ceramics

Rongquan Duan,[†,‡] Davide Barbieri,[†,‡] Florence de Groot,[‡] Joost D. de Bruijn,[†,‡,§] and Huipin Yuan*[,‡,∥,⊥]

[†]Biomaterial Science and Technology, MIRA, University of Twente, 7522 NB Enschede, The Netherlands

[‡]Kuros Biosciences BV, 3723 MB Bilthoven, The Netherlands

[§]School of Engineering and Materials Science, Queen Mary University of London, London E1 4NS, U.K.

[∥]MERLN Institute for Technology Inspired Regenerative Medicine, Maastricht University, 6200 MD Maastricht, The Netherlands

[⊥]College of Physical Science and Technology, Sichuan University, Chengdu 610064, China

ABSTRACT: Tricalcium phosphate (TCP) ceramics are used as bone void fillers because of their bioactivity and resorbability, while their performance in bone regeneration and material resorption vary with their physical properties (e.g., the dimension of the crystal grain). Herein, three TCP ceramic bone substitutes (TCP-S, TCP-M, and TCP-L) with gradient crystal grain size (0.77 ± 0.21 μm for TCP-S, 1.21 ± 0.35 μm for TCP-M and 4.87 ± 1.90 μm for TCP-L), were evaluated in a well-established rabbit lateral condylar defect model (validated with sham) with respect to bone formation and material resorption up to 26 weeks. Surface structure-dependent bone regeneration was clearly shown after 4 weeks implantation with TCP-S having most mineralized bone (20.2 ± 3.4%), followed by TCP-M (14.0 ± 3.5%), sham (8.1 ± 4.2%), and TCP-L (6.6 ± 2.6%). Afterward, the amount of mineralized bone was similar in all the three groups, but bone marrow and material resorption varied. After 26 weeks, TCP-S induced most bone tissue formation (mineralized bone + bone marrow) (61.6 ± 7.8%) and underwent most material resorption (80.1 ± 9.0%), followed by TCP-M (42.9 ± 5.2% and 61.4 ± 8.0% respectively), TCP-L (28.3 ± 5.5% and 45.6 ± 9.7% respectively), and sham (25.7 ± 4.2%). Given the fact that the three ceramics are chemically identical, the results indicate that the surface structure (especially, the crystal grain size) of TCP ceramics can greatly tune their bone regeneration potential and the material resorption in rabbit condyle defect model, with the submicron surface structured TCP ceramic performing the best.

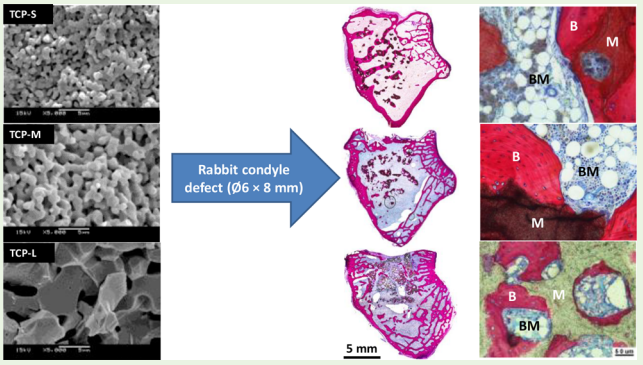

KEYWORDS: *bone substitutes, beta-tricalcium phosphate, crystal grain size, bone formation, material resorption*

1. INTRODUCTION

In orthopedic surgery, autograft is still the golden standard to treat critical-sized bone defects. However, its drawbacks such as complications and limited availability drove the development of synthetic bone substitutes.[1−3] Thanks to their chemical similarity to the inorganic component of bone and teeth, biocompatibility, bioactivity, and osteoconductivity, calcium phosphate (CaP) ceramics including beta-tricalcium phosphate (β-TCP), hydroxyapatite (HA), and biphasic calcium phosphate (BCP) are often considered as bone grafting materials, either alone or as autograft extenders.[4−7]

Despite that osteoconductive CaP ceramics could conduct bone formation, the conductive bone is restricted to areas nearby the host bone bed, limiting their clinical application in the repair of critical-sized bone defects.[8,9] However, a subgroup of CaP ceramics with special physicochemical properties was found to trigger bone formation, that is, osteoinduction, in heterotopic sites (e.g., intramuscular or subcutaneous).[10−12]

When tested in the ectopic implantation models, the bone-forming potential of CaP ceramics varied with their physicochemical properties.[13−19] For instance, bone formation in CaP ceramics was affected by the HA/TCP ratio in intramuscular implantation models.[13,14] In addition to the chemistry, CaP ceramic-directed bone formation in ectopic sites depended largely on physical factors (e.g., macroporosity,[10−12] microporosity,[15,16] and the dimension of surface crystal grain[17−19]). In particular, without any osteogenic additives, the reduction of the dimension of the surface crystal grain could render CaP ceramics osteoinductive.[17−19] For example, a BCP ceramic with small crystal size and large amount of micropores induced bone formation in muscle of goats, while the one having larger crystal size and fewer micropores did not.[13] The importance of surface structure in

Received: May 30, 2018
Accepted: July 26, 2018
Published: July 26, 2018

DOI: 10.1021/acsbiomaterials.8b00630
ACS Biomater. Sci. Eng. 2018, 4, 3347−3355

material-driven osteoinduction was clearly shown in studies, where TCP ceramic having submicron surface crystal grains triggered bone formation in muscles while micron surface structured TCP failed.[17−19]

Although material-driven osteoinduction is animal-dependent,[20] CaP ceramics with submicron surface crystals led to ectopic bone formation in goats,[13] canines,[17−19] and FVB mice.[21] Meanwhile, these submicron-scaled surface structured CaP ceramics enhanced bone regeneration in the iliac crest of goats[22] and the spine of beagles.[23] Furthermore, such osteoinductive CaP ceramics were as good as autograft and outperformed a nonosteoinductive CaP ceramic in ovine critical-sized iliac wing defects.[24]

In addition to serving as a temporary scaffold to facilitate bone regeneration, an ideal bone substitute should gradually degrade during the bone remodeling process and ultimately be replaced by the newly formed bone.[25,26] It is well-known that resorption rate of CaP ceramics could be chemically controlled by the means of HA/TCP ratio. β-TCP is of major interest and is often used in clinics because of its higher resorption rate.[27,28] Next to its chemistry, the resorption rate of TCP ceramic is affected by the physical properties (e.g., the dimension of the surface architecture). For instance, functional osteoclast-like cells could form on the TCP surfaces with submicron crystal grains but not on those with micron scale crystal grains. As a result, TCP ceramics with submicron crystal grains were more resorbable as compared with their counterparts with micron-scale grains following an intramuscular implantation.[17−20]

Given the fact that the crystal grain size largely impacted the bone forming potential and resorption rate of TCP ceramic in ectopic sites, it is assumed that the performance of such TCP ceramics varies also in orthotopic sites. In this study, we selected three TCP ceramics with gradient crystal grain size and made comparisons in a well-established rabbit lateral condylar defect model with respect to bone regeneration and material resorption.[29,30]

2. MATERIALS AND METHODS

2.1. Preparation of TCP Ceramics. TCP-M (Osferion, Olympus, 1.0−3.0 mm) and TCP-L (chronOS, Synthes, 1.4−2.8 mm) were purchased and used as received. TCP-S was prepared as previously described elsewhere.[24] In brief, phosphoric acid solution (H_3PO_4, Fluka, Steinheim, Germany) was added dropwise to a calcium hydroxide suspension ($Ca(OH)_2$, Fluka) at a Ca/P ratio of 1.5. After aging at room temperature for 6 weeks, the slurries were filtered, and TCP-S powder was eventually obtained after drying and grinding. This powder was then foamed with diluted H_2O_2 (1% in distilled water, Merck, Darmstadt, Germany) and a porogen (wax particles, 600−1000 μm, Merck) at 60 °C to get green bodies. TCP-S ceramic was finally obtained by sintering the green bodies at 1050 °C for 8 h. Irregularly shaped granules (1.0−2.0 mm) were prepared by crushing the sintered bodies and sieving. The granules were then ultrasonically cleaned with acetone (Fluka), 70% ethanol (Fluka) and demineralized water, dried at 80 °C, and sterilized with gamma irradiation (dose 25−40 kGy, Isotron Netherlands B.V., Ede, The Netherlands) prior to use.

2.2. Physicochemical Characterization. The chemistry of the TCP ceramics was characterized by X-ray diffraction (XRD; Miniflex II, Rigaku, Tokyo, Japan). The surface structure was evaluated with scanning electron microscope (SEM; XL30, ESEM-FEG, Philips, Eindhoven, The Netherlands) where 100 crystal grains were randomly selected from 10 SEM images (5000×) and were measured with AxioVision LE (Carl Zeiss MicroImaging, Inc., Breda, The Netherlands). The pore size distribution in the ceramic strut and the surface area of the ceramics were obtained with mercury intrusion (n = 1 per material, Micromeritics Instrument Incorporation, Norcross, GA, U.S.A.).

2.3. Protein Adsorption in Vitro. Ceramic granules (0.2 cc, n = 6) were soaked into 2 mL of medium composed of minimal essential medium-alpha (a-MEM; Gibco, Invitrogen, U.K.) supplemented with 10% fetal bovine serum (FBS, Lonza, Germany) and 1% penicillin/streptomycin (Gibco, Invitrogen, U.K.), and incubated at 37 °C in a humid atmosphere with 5% CO_2 for 4 days. After washing three times with phosphate buffer solution (PBS, Invitrogen, Darmstadt, Germany), 0.5 mL of 1% Triton solution was added to each sample. Thereafter the amount of protein detached from the samples into the Triton solution was measured with the QuantiPro BCA Assay Kit (Pierce Biotechnology Inc., Rockford, U.S.A.) following the manufacturer's instructions, and absorbance was measured with a spectrophotometer (Anthos Zenyth 3100, Anthos Labtec Instruments GmbH, Salzburg, Austria) at 620 nm. A calibration curve was prepared using standard FBS solutions. The amount of proteins adsorbed onto the ceramics was then converted to the same amount of the material (1.0 cc) and expressed as mean ± SD.

2.4. Calcium and Phosphate Ion Release. Calcium and phosphate ion release from the ceramics was determined by placing 0.5 cc of ceramic granules (n = 3) in 100 mL of simulated physiological saline (SPS; 0.8% NaCl, 50 mM HEPES, 0.4 mM NaN_3, 37 °C, pH = 7.3) for 1, 4, and 7 days. The calcium and phosphate ion concentrations in the SPS solution were measured with a QuantiChrom Calcium assay kit (BioAssay Systems, Hayward, U.S.A.) and a PhosphoWorks Colorimetric Phosphate assay kit (AAT Bioquest, Inc., Sunnyvale, U.S.A.), respectively, following the manufacturer's guidelines. Absorbances were measured with the spectrophotometer at 620 nm. The calcium and phosphate ion concentrations were quantified respectively with the respective standard calibration curves and expressed as mean ± SD.

2.5. Animal Experiment. A total of 36 New Zealand white rabbits (female, 6 months, 3.5−4.5 kg) were used for this study. Rabbits were housed separately in stainless steel cages in laboratory animal at 20−25 °C with 50−60% humidity, and a light cycle coinciding with daylight hours. They were acclimatized to their new housing facilities for 2 weeks before surgery. Operations were performed with the permission of the local animal ethic committee (the Management Committee of Experimental Animals of Sichuan Province, China) under general sterile conditions. All surgeries were conducted under general anesthesia by intravenous injection of sodium pentobarbital (30 mg kg^{1-} body weight; Merck) in the marginal ear vein of rabbits. One defect (Ø6 × 8 mm) was created on each lateral condyle. In brief, a longitudinal skin incision of 3 cm was made on the lateral femoral condyle, which was exposed following the entire removal of the overlying periosteum. At this point, a 2.0 mm pilot hole was generated with a drill (Ø = 2 mm) perpendicular to the long axis of the femoral shaft, and then the pilot hole was gradually widened with a larger drill (Ø = 6 mm) eventually creating a critical-sized defect (Ø6 × 8 mm). Both lateral femoral condyles of each rabbit were operated, and each defect was either randomly treated with one of the three CaP ceramic granules until the defect was completely filled (n = 6 per group), or was left untreated (sham, n = 6). Afterward, the muscle and skin were closed layer by layer with sutures in a routine surgical manner.

After surgery, the animals were intramuscularly given buprenorphine (0.1 mg per animal, Merck) for 2 days to relieve pain and penicillin (40 mg kg^{-1}; Merck) for 3 consecutive days to prevent infection. Animals were fed ad libitum and were allowed to move inside their cages without restriction. At each postoperative time interval (i.e., 4, 12, and 26 weeks after implantation), 12 rabbits were sacrificed with a marginal ear vein injection of excessive amount of sodium pentobarbital, and samples were harvested for the radiographic analysis and histological evaluation.

2.6. Radiographic Examination. After stripping away the soft tissues, the femoral condyles were fixed in formaldehyde solution for 3 days, and then the bone defects were evaluated with X-ray radiography in the sagittal plane by three people in a blinded fashion. The conclusions were drawn on the basis of the gray level differences

DOI: 10.1021/acsbiomaterials.8b00630
ACS Biomater. Sci. Eng. 2018, 4, 3347−3355

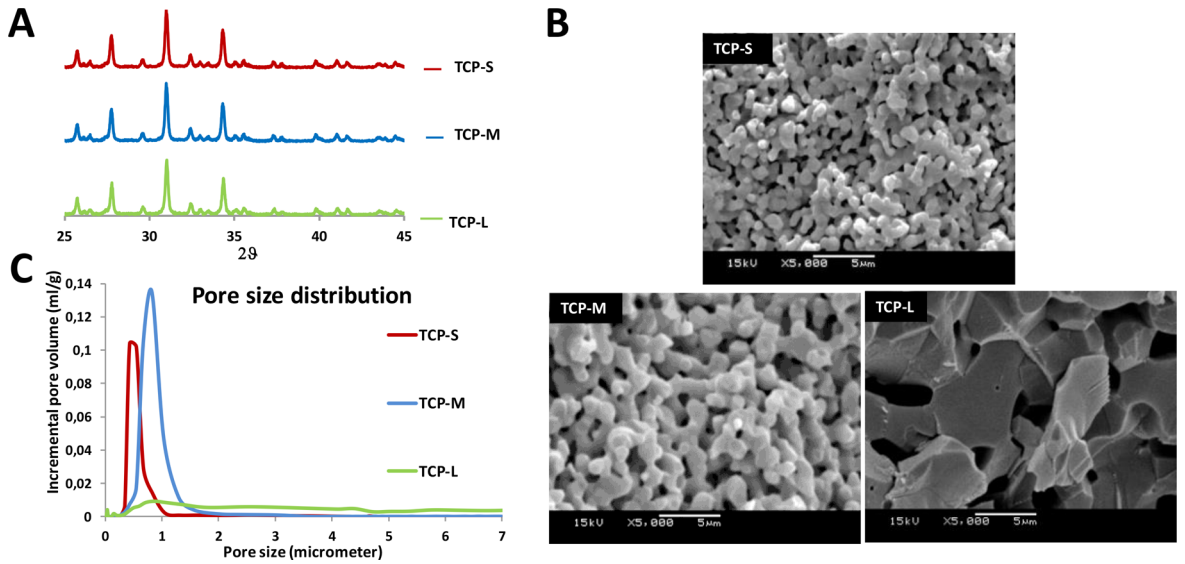

Figure 1. (A) XRD pattern showing that the chemistry of the three TCP ceramics is β-TCP; (B) SEM images show that the three TCP ceramics have different surface crystal grain size; (C) Distribution plots of the surface pore dimension.

Table 1. Physicochemical Properties of CaP Ceramics

materials	suppliers	chemistry[a]	particle size (mm)	strut pore size[b]	surface grain size[c] (μm)	strut porosity[b] (%)	specific surface area (by weight)[b] ($m^2\ g^{-1}$)	specific surface area (by volume)[b] ($m^2\ mL^{-1}$)
TCP-S	homemade	β-TCP	1.0−2.0	submicron	0.77 ± 0.21	45.14	1.87	1.62
TCP-M (Osferion)	Olympus	β-TCP	1.0−3.0	submicron	1.21 ± 0.35	51.90	1.47	1.28
TCP-L (chronOS)	Synthes	β-TCP	1.4−2.8	micron	4.87 ± 1.90	31.52	0.51	0.59

[a]as evaluated by X-ray diffractometry. [b]obtained from mercury intrusion. [c]as confirmed by quantitative measurements on scanning microscopic images (5000×).

between ceramic and bone tissue, and the consequent change of gray level distribution in the defects with implantation time.

2.7. Histological Evaluation. After radiographic examination, all explants were trimmed as much as possible without harming the host bone surrounding the implants and embedded in methyl methacrylate (MMA) after dehydration with a series of ethanol solutions. The embedded samples were trimmed and mounted on a diamond saw microtome (Leica SP-1600, Wetzlar, Germany). Three nondecalcified sections (10−20 μm) were made crossing the middle of each explants (on the axial plane) and stained with 1% methylene blue (Sigma-Aldrich, St, Louis, MO) and 0.3% basic fuchsin (Sigma-Aldrich) for light microscope observation. All the stained sections were digitalized with a scanner (Dimage Scan Elite5400 II, Konica Minolta, Tokyo, Japan) to obtain overview images for the quantification of the de novo bone formation and material resorption. The analysis was performed by pseudocoloring pixels representing mineralized bone (MB), bone marrow (BM), soft tissue (ST), and the remaining material (Me) in the region of interest (ROI, a 5 × 5 mm square overlapping the center of the defect) using Adobe Photoshop software (CS5, v12, Adobe Systems Benelux BV, Amsterdam-Zuidoost, The Netherlands). The Me%, MB%, BM%, bone tissue%, and ST% were calculated as follows:

$$\text{Me\%} = \text{Me} \times 100/\text{ROI}$$

$$\text{MB\%} = \text{MB} \times 100/\text{ROI}$$

$$\text{BM\%} = \text{BM} \times 100/\text{ROI}$$

$$\text{bone tissue\%} = \text{MB\%} + \text{BM\%}$$

$$\text{ST\%} = (\text{ROI} - \text{Me} - \text{bone tissue}) \times 100/\text{ROI}$$

The ST includes fibrous tissues as well as blood vessels.

The resorption rate of the ceramics was calculated as (Mi% − Me %) × 100/Mi%, where the initial area percentage of the ceramic material (Mi%) in the implants was determined after making 10−20 μm thick sections (ROI, a 5 × 5 mm) of MMA-embedded nonimplanted ceramic granules (0.2−0.3 mL, n = 6).

2.8. Statistical Analysis. Statistical analysis was carried out using one-way analysis of variance (ANOVA) with Tukey's test ($p < 0.05$ for statistically significant differences), while normality of the data was assessed using the Shapiro-Wilk test ($p > 0.05$ for normally distributed data). The power of all experiments was determined with a posthoc statistical power analysis (one-way omnibus ANOVA test with fixed effects).

3. RESULTS

3.1. Physicochemical Properties of the TCP Ceramics. The XRD patterns of the CaP ceramics are given in Figure 1A, which shows that the three CaP ceramics are chemically equivalent and belong to β-TCP. SEM images showed that the three CaP ceramics had gradient crystal grain size as expected (Figure 1B), with crystal grain size of 0.77 ± 0.21 μm for TCP-S, 1.21 ± 0.35 μm for TCP-M and 4.87 ± 1.90 μm for TCP-L (Table 1). The microporosity was affected by both the number and the size of micropores and varied with materials (Figure 1B, Table 1). TCP-M had slightly higher strut porosity (51.90%) compared with TCP-S (45.14%), while TCP-L had the lowest strut porosity (31.52%). As also shown in Figure 1C, the micropores were mainly 0.3−1.0 μm in size for TCP-S, 0.5−1.5 μm for TCP-M and 0.5−7.0 μm for TCP-L. TCP-S also had the highest specific surface area by volume (1.62 m^2

DOI: 10.1021/acsbiomaterials.8b00630
ACS Biomater. Sci. Eng. 2018, 4, 3347−3355

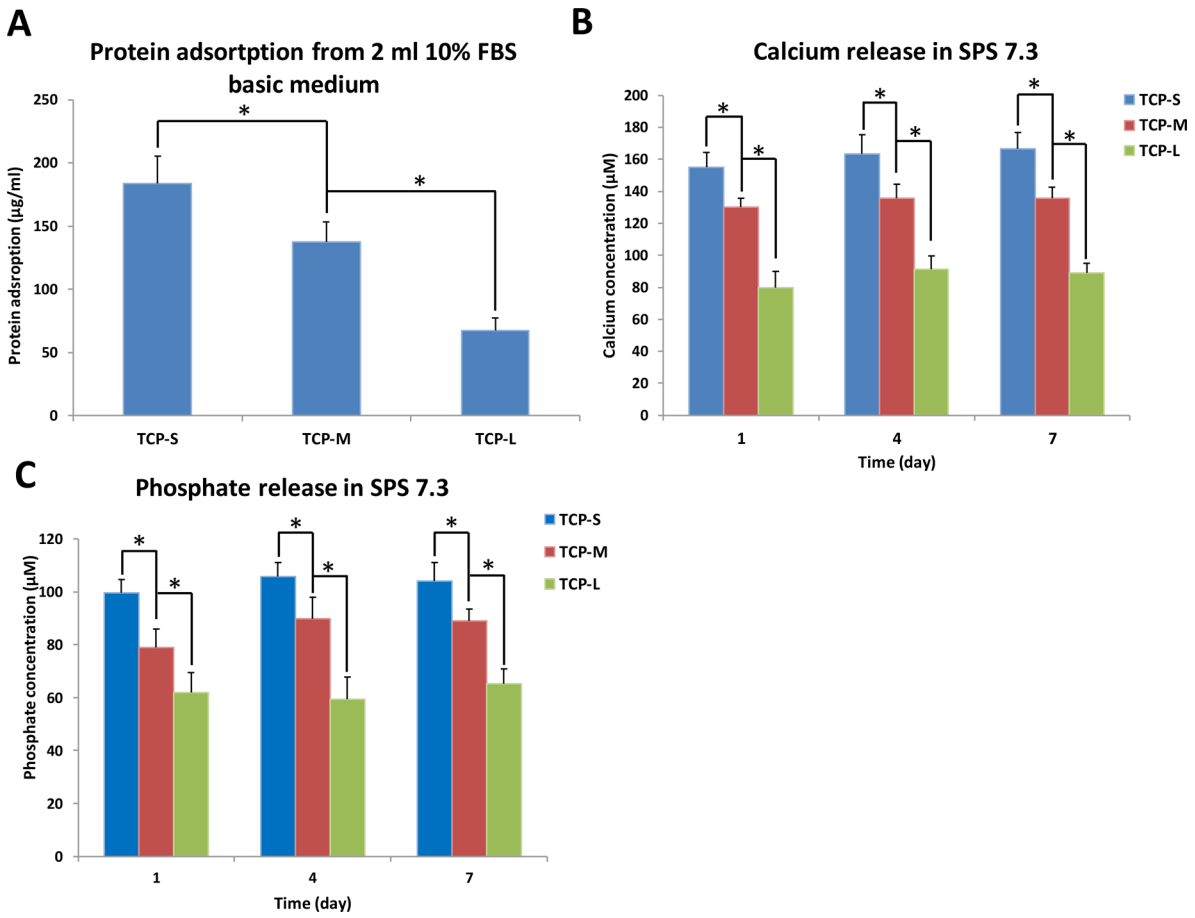

Figure 2. (A) Amount of protein adsorbed into implants (1 mL) from basic medium after 4-day incubation; (B,C) Calcium and phosphate ions release from the materials into SPS at day 1, day 4, and day 7 (stars indicate a statistically significant difference, $p < 0.05$). For all the three experiments, the Shapiro–Wilk normality test gave $p > 0.05$. The power (and effect size) were 1.00 (2.95), 1.00 (3.74), and 0.99 (1.74) for protein adsorption, calcium and phosphate ion release experiments, respectively.

mL^{-1}) followed by TCP-M (1.28 m^2 mL^{-1}) and TCP-L (0.59 m^2 mL^{-1}) (Table 1).

3.2. Protein Adsorption in Vitro. After the ceramics were soaked in culture medium containing FBS for 4 days, the amount of protein adsorption by CaP ceramics was correlated to their specific surface area (Figure 2A and Table 1). TCP-S with the largest specific surface area adsorbed significantly more protein (183.9 ± 21.7 μg mL^{-1}), followed by TCP-M (137.3 ± 15.7 μg mL^{-1}) and TCP-L (67.1 ± 10.4 μg mL^{-1}).

3.3. Calcium and Phosphate Ion Release. The amount of calcium ions released by the three CaP ceramics is shown in Figure 2B. TCP-S released the most calcium ions into SPS 7.3 solution (155.1 ± 9.2 μM, 163.3 ± 12.2 μM and 166.6 ± 10.3 μM at 1, 4, and 7 days, respectively), followed by TCP-M (130.1 ± 5.7 μM, 135.8 ± 8.8 μM and 135.7 ± 6.8 μM at 1, 4, and 7 days, respectively) and TCP-L (79.6 ± 7.4 μM, 91.5 ± 8.3 μM, and 88.9 ± 5.9 μM at 1, 4, and 7 days, respectively). Similarly, as shown in Figure 2C, TCP-S also released the most phosphate ions into SPS 7.3 solution, followed by TCP-M and TCP-L. Differences among materials were statistically significant at all end points; however, ion release did not increase with soaking time.

3.4. Radiographic Examination. As shown in the X-ray images (Figure 3), 4 weeks after implantation the three materials were observed in the defects because of their higher radiologic density compared to the adjacent cancellous bone.

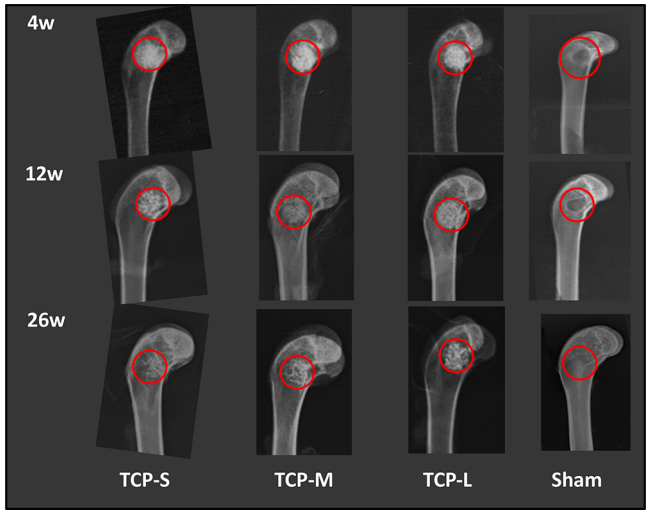

Figure 3. X-ray photos of the rabbit condylar defects with TCP-S, TCP-M TCP-L and sham ranging from 4 to 26 weeks postoperatively.

In particular, the margins between the adjacent bone and the defects filled with TCP-S and TCP-M were already indistinct, indicating that the implanted materials were well incorporated with the surrounding bone. On the contrary, the margin of the sham and defects treated with TCP-L were still clearly visible, indicating no closure. At 12 weeks, the contour of all the

DOI: 10.1021/acsbiomaterials.8b00630
ACS Biomater. Sci. Eng. 2018, 4, 3347–3355

implanted materials became vaguer and most likely was continuously replaced by de novo bone; meanwhile, the defects treated with sham were still not fully closed. At 26 weeks, the TCP-S implants almost disappeared, and the defects had similar gray levels to the cancellous bone, followed by TCP-M. Indeed, the resorption and material replacement with bone in TCP-L was markedly delayed as the material was still clearly recognized in the defects. A partial closure of sham defects was visible.

3.5. Histological Evaluation in Summary. As shown in the histological overviews after 4 weeks (Figure 4), a considerable creeping MB had been penetrated well into the whole defects treated with TCP-S, and relatively less MB was observed at the defect margins in TCP-M implants. In defects filled with TCP-L, limited MB was restricted to peripheral regions close to the host bone bed, and no bone tissue could be observed in the center of the defects. In addition, the ceramic material within the defects was still largely intact in all three materials.

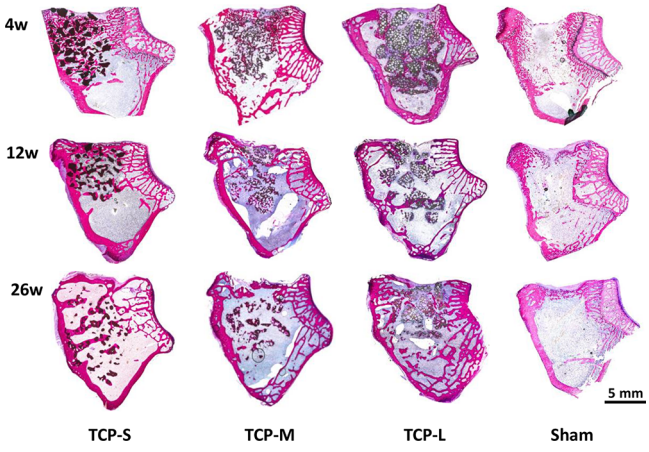

Figure 4. Histological overviews showing the bone regeneration and material resorption within condylar defects of rabbits ranging from 4 to 26 weeks postoperatively (undecalcified sections stained with methylene blue and basic fuchsin, where bone was stained fresh-red).

After 12 weeks, the bone tissue (consisting of MB and BM) increased continuously within the defects treated with all three ceramics. The MB increased within defects implanted with TCP-M and TCP-L, but was significantly decreased in those treated with TCP-S (where much MB was remodeled into BM). Meanwhile, the amount of the residual materials decreased as compared with the earlier end point. In addition, the condyle defects treated with TCP-S were closed by the newly formed bone (6/6), while those treated with TCP-M, TCP-L, and sham were partially repaired, and no full repair was achieved in any of the defects.

By 26-week postoperatively, de novo bone formation, bone remodeling, and material resorption were continuously proceeding within the defects containing ceramics. An increase of MB was noted in condyle defects with TCP-L. Bone remodeling primarily dominated with the evidence of decreased MB and increased BM in those defects treated with TCP-S and TCP-M. A limited amount of resident ceramic was observed in the center of the defects filled with TCP-S, while more was seen in the TCP-M group. The TCP-L material was still predominantly present in the defects. In addition, defects treated with TCP-M were now completely closed with new bone (6/6), but defects treated with TCP-L and sham were still open (6/6).

3.6. Histological Evaluation in Detail. Examination with light microscopy revealed the presence of normal bony structures with osteocytes embedded in the lacunae and osteoblasts lining de novo bone after 4 weeks of treatment in all three groups. However, BM was detected only in TCP-S, while the space in defects treated with TCP-M and TCP-L was generally occupied by loose connective tissue. Additionally, numerous phagocytic cells colonized the surface of TCP-S and phagocytized ceramic debris. Limited phagocytes adhered on TCP-M surfaces and was rarely noted on TCP-L surfaces; additionally, the sham consisted of much soft tissue and limited MB (Figure 5).

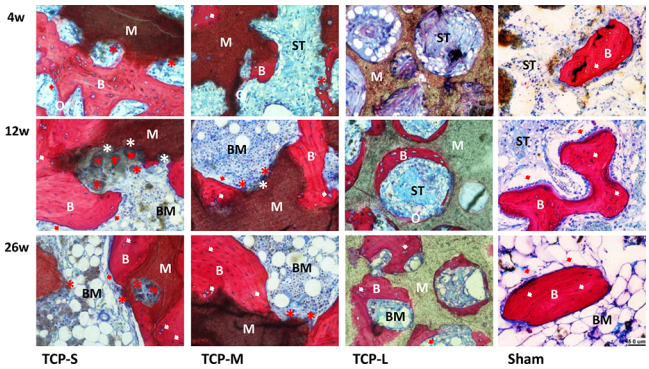

Figure 5. Light microscope images taken in the central of the defects showing bone formation, bone remodeling, and degradation of CaP ceramics implanted in condylar defects of rabbits ranging from 4 to 26 weeks postoperatively (undecalcified sections stained with methylene blue and basic fuchsin, B: bone; O: osteoid; M: material; BM: bone marrow; ST: soft tissue; red arrows: osteoblasts; white arrows: osteocytes; red asterisks: phagocytic cells; white asterisks: scalloped structures of ceramics).

After 12 weeks of implantation, the bone regeneration and remodeling continuously proceeded with the evidence of BM increase in TCP-S and TCP-M, and MB increase in TCP-L (Figure 5). Meanwhile, higher phagocytic activity in TCP-S than in TCP-M and TCP-L was seen as phagocytes engulfed particles, and there was scalloped structure formation on the ceramic surfaces.

After 26 weeks of implantation, MB was remodeling into cancellous bone, BM was seen in all three implants as well as in sham, and osteoblast-like cells were rarely seen in the center. When such cells were seen, they were much flatter than those at 12 weeks. In addition, the number of phagocytes attached on the TCP-S and TCP-M surface decreased compared with those seen at the 12-week end point, while the phagocytes were still rarely seen on TCP-L.

3.7. Quantitative Histology. At the 4-week postoperative time interval, most MB were noted in defects treated with TCP-S (20.2 ± 3.4%) and followed by TCP-M (14.0 ± 3.5%), sham (8.1 ± 4.2%), and TCP-L (6.6 ± 2.6%). By 26 week postsurgery, TCP-S gave rise to most bone tissue formation (61.6 ± 7.8%), followed by TCP-M (42.9 ± 5.2%) and TCP-L (28.3 ± 5.5%) and sham (25.7 ± 4.2%). Quantification of the absolute percentage of ceramic residuals within the defect showed that the most resorption occurred in TCP-S (80.1 ± 9.0%), followed by TCP-M (61.4 ± 8.0%) and TCP-L (45.6 ±

DOI: 10.1021/acsbiomaterials.8b00630
ACS Biomater. Sci. Eng. 2018, 4, 3347−3355

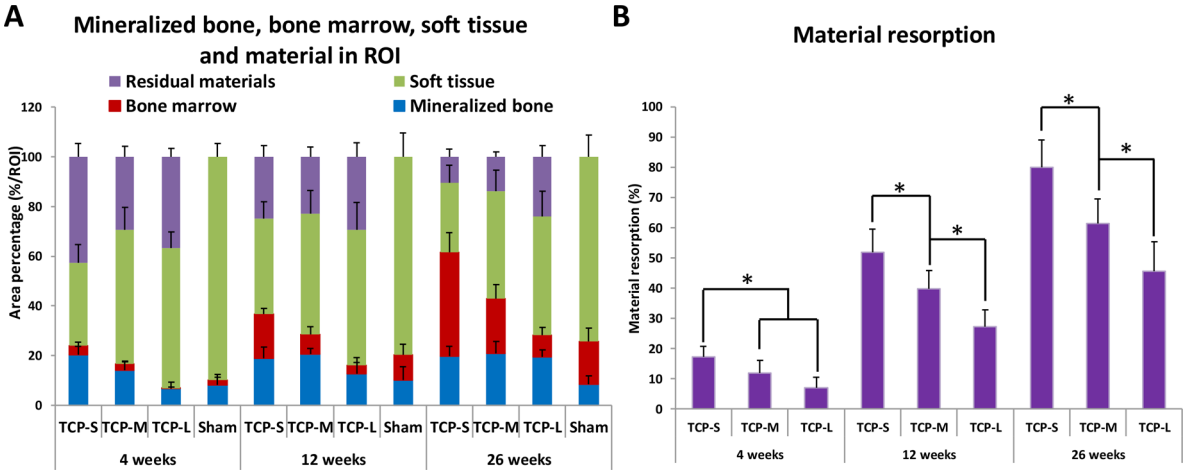

Figure 6. Quantitative histomorphometry data on (A) the area percentage of mineralized bone, bone marrow, other soft tissue and residual material in ROI, and (B) the material resorption rate ranging from 4 to 26 weeks postoperatively (stars indicate a statistically significant difference, $p < 0.05$). For all three experiments, the Shapiro–Wilk normality test gave $p > 0.05$. The power (and effect size) were 1.00 (3.90) and 1.00 (3.62) for bone tissue and resorption experiments, respectively.

9.7%) (Figure 6). Differences in total bone tissue between materials were always statically significant at all end points.

4. DISCUSSION

This study aimed at evaluating the bone regeneration and material resorption as a function of crystal grain size of TCP ceramics in a well-established rabbit lateral condylar defect model. The main finding was that the three TCP ceramics had different bone regeneration potential and underwent resorption at different rates according to the crystal grain size.

4.1. Bone Regeneration. Although each had different rates, the newly formed bone tissue increased with the implantation time for all the three TCP ceramics. As shown in Figure 4, the most de novo MB occurred throughout TCP-S implants at 4-week postoperative time interval, followed by TCP-M and TCP-L where limited MB was restricted in peripheral areas adjacent to the host bone. Afterward, the amount of MB was comparable in the three groups, but the BM, which indicates ongoing bone remodeling, varied among the three implanted materials (TCP-S > TCP-M > TCP-L), resulting in a direct relationship between bone tissue (BM +MB) and the crystal grain size. Bone regeneration in osseous sites could be formed both by inducible mesenchymal stem cells via osteoinduction and by osteogenic cells via osteoconduction. In our previous study, following intramuscular implantation in beagles, TCP-S could induce significantly more ectopic bone formation (21%) than TCP-M (8%), while TCP-L with micron scaled surface did not trigger any bone formation.[19] Therefore, the enhanced bone regeneration and remodeling in TCP-S implants should be the result of both the enhanced conductive bone formation in regions close to the host bone and the inductive bone formation in the central area of the implants.[17−19,23]

Indeed, it has been shown that a specific surface topography, which occurred as a result of the combination of different dimensions of crystal grains and micropores with the microporosity, could tune adherent cell fate through mechanotransduction.[19,21,31−34] More specifically, the surface structure with a range from nano- to microscale could profoundly influence the cellular orientation, attachment, proliferation, and differentiation irrespectively of the chemistry, even without osteogenic additives.[33−41] In the current study, TCP-S with crystal grains and micropores at the submicron scale constructed a specific surface topography, which directly affected the osteogenic differentiation of inducible mesenchymal stem cells (osteoinduction) and the osteogenesis of bone forming cells (osteoconduction) in orthopedic sites. As a result, bone regeneration in condyle defects treated with TCP-S was enhanced. This conclusion is also supported by our previous work, where TCP-S was osteoinductive in an ectopic site[19,23] and enhanced bone regeneration in the spine.[23]

In addition to the surface topography, the increase of microporosity and the concomitant decrease of crystal grain and micropore dimensions augmented the surface area of CaP ceramics. The enlarged surface area of TCP-S could have entrapped and concentrated more proteins (e.g., BMP) than TCP-M and TCP-L, which could have later induced the differentiation of undifferentiated cells to achieve osteogenesis favoring bone formation.[41−44] At the same time, calcium and phosphate ion release was related to the physical properties of the ceramics (e.g., surface area and crystallinity). Thus, the enlarged surface area of TCP-S could have provided a richer calcium ion microenvironment, which is not only a source for the building blocks of bone but could also enhance the proliferation, osteogenic differentiation, and mineralization of bone-forming cells to finally synthesize bone matrix.[45,46] Conversely, TCP-L with the largest crystal grains and lowest microporosity had the least surface area and formed the least bone. It appeared that the influence of crystal grain size on the bone forming potential of CaP ceramics could be attributed to the surface area that tunes protein adsorption and ion release.

Among the factors affecting bone regeneration with CaP ceramics, the size and interconnectivity of macropores (pores >50 μm) are important ones.[10−12] The macropores inside the individual particles were interconnected, as evidenced by the presence of infiltrated tissues in the pores (Figure 5). Because the three materials studied here had similar particle size range (1.0−3.0 mm, Table 1), they could have similar macroporosity and fully connected microporous structures after being packed in the defects. Therefore, the influence of pores larger than 50 μm on bone formation between the three groups could be minimized in this study.

DOI: 10.1021/acsbiomaterials.8b00630
ACS Biomater. Sci. Eng. 2018, 4, 3347−3355

4.2. Material Resorption. Similarly to ectopic implantation model, the resorption of TCP ceramics varied with the crystal grain size in osseous site. The finer the crystal grains, the faster resorption was seen. TCP-S had the highest rate of resorption, followed by TCP-M and TCP-L (Figure 6B).

The resorption of CaP ceramics was suggested to involve two types of processes: solution-mediated disintegration (i.e., passive dissolution) and cell-mediated resorption.[47,48] It has been suggested that increasing the surface area could enhance the contact between the ceramic and the surrounding body fluids rendering the material more prone to passive dissolution.[23] As shown in Figure 2B, TCP-S released the most calcium ions indicating that it dissolved faster than TCP-M and TCP-L due to its larger surface area (Table 1). In addition, cell-mediated resorption has been proven to play important roles in the resorption of CaP ceramics in vivo, where typical osteoclastic resorption pits on CaP ceramic surface were observed.[49] As shown in detailed histological images at the 12-week time period, a number of multinucleated osteoclast-like cells colonized the surface of TCP-S phagocytizing material fragments and scalloping much surface (Figures 5), which indicates an active cell-mediated material resorption. A limited amount such phagocytes and scalloped structure surface were detected in TCP-M. Conversely, such resorbing cells were missing in TCP-L implants (Figure 6B). Indeed, it has been shown that the surface structure dimension greatly affected the cell-mediated resorption of TCP ceramics, via the differential formation of multinucleated osteoclast-like cells and resorption capacity of osteoclasts. For example, TCP with a submicron-scale surface structure not only enhanced the formation of osteoclasts from mononuclear cells, but it was also resorbed by the osteoclasts formed on the surface, as compared with its micron-scale surface structured counterpart.[50] In this study, having a larger surface area facilitating chemical dissolution and the right surface structure, which is suitable for the formation and function of osteoclasts, and the submicron surface structure may have enhanced the resorption of TCP-S ceramic.

4.3. Bone Remodeling and Material Resorption. When comparing the bone regeneration and material resorption, the resorption of the three TCP ceramics in osseous sites appeared to be coupled with bone remodeling. Bone tissue consisting of MB plus BM increased with time, ranging from 4 to 26 weeks poste-operatively, in all the three groups (Figure 6A). The mineralized bone in TCP-S reached its peak at week 4 and decreased thereafter with no significant difference to TCP-M and TCP-L at week 12 and week 26. However, at week 12 and 26, significantly more BM was formed in TCP-S than in TCP-M and TCP-L. This result is in line with that previously demonstrated,[13,14,17,24] as TCP-S with the specific surface architecture enhanced the formation of osteoclasts. This fact not only enhanced the material resorption, but it also facilitated the remodeling of the bone formed at the early end points. Thus, more bone marrow could be detected in TCP-S, while TCP-L with micron-scale surface structure did not favor osteoclast generation and underwent the less material resorption and bone remodeling. The group of TCP-M has a performance between TCP-S and TCP-L.

The results obtained in this study demonstrate that, despite the same chemical composition, the bone regeneration capacity and resorption of CaP ceramics were different. Physical properties, especially the crystal grain size, are important in determining the functionality of CaP ceramics in bone regeneration and remodeling, and in material resorption in rabbit condyle defect model.

These finding may provide scientists clues for further optimization of CaP ceramic bone substitutes and would be helpful for clinicians in selecting the right CaP ceramic bone substitutes for bone regeneration. However, studies with larger critical-size defects (e.g., iliac crest defect Ø = 17 mm) and functional studies (e.g., posterolateral lumbar fusion) would be necessary to further confirm the function of submicron-scale surface structured calcium phosphate ceramics.

5. CONCLUSIONS

When three TCP ceramics with various dimensions of crystal grains were compared in rabbit femoral condyle defects for up to 26 weeks, the influence of surface structure scale on bone regeneration and material resorption was shown. Submicron structured TCP-S gave rise to most bone formation and underwent most resorption as compared to TCP ceramics with larger crystal grains. The data could be useful for further optimizing CaP ceramic bone substitutes and selecting the most suitable CaP ceramic bone substitutes for clinical application.

AUTHOR INFORMATION

Corresponding Author

*Fax: 0031-30-2297299. Tel.: 0031-30-2297292. E-mail: h.yuan@maastrichtuniversity.nl.

ORCID

Rongquan Duan: 0000-0003-0728-8337

Notes

The authors declare no competing financial interest.

ACKNOWLEDGMENTS

The authors would like to thank the Seventh Framework Programme of the European Union (REBORNE under grant agreement no. 241879), The Netherlands Institute for Regenerative Medicine (NIRM) and Rapid Prototyping of Custom-Made Bone-Forming Tissue Engineering Constructs (RAPIDOS Project, ref. NMP-2013-EU-China604517), and the Horizon 2020 Framework Programme (CHARME, grant agreement no. 674282) for their financial support in this study.

REFERENCES

(1) García-Gareta, E.; Coathup, M. J.; Blunn, G. W. Osteoinduction of bone grafting materials for bone repair and regeneration. *Bone* **2015**, *81*, 112−121.

(2) Roberts, T. T.; Rosenbaum, A. J. Bone grafts, bone substitutes and orthobiologics: the bridge between basic science and clinical advancements in fracture healing. *Organogenesis* **2012**, *8*, 114−124.

(3) Zhang, J.; Liu, W.; Schnitzler, V.; Tancret, F.; Bouler, J. M. Calcium phosphate cements for bone substitution: chemistry, handling and mechanical properties. *Acta Biomater.* **2012**, *10*, 1035−1049.

(4) Habraken, W.; Habibovic, P.; Epple, M.; Bohner, M. Calcium phosphate in biomaterial applications: materials for the future. *Mater. Today* **2016**, *19*, 69−87.

(5) Khan, A. F.; Saleem, M.; Afzal, A.; Ali, A.; Khan, A.; Khan, A. R. Bioactive behavior of silicon substituted calcium phosphate based bioceramics for bone regeneration. *Mater. Sci. Eng., C* **2014**, *35*, 245−252.

(6) Samavedi, S.; Whittington, A. R.; Goldstein, A. S. Calcium phosphate ceramics in bone tissue engineering: a review of properties and their influence on cell behavior. *Acta Biomater.* **2013**, *9*, 8037−8045.

DOI: 10.1021/acsbiomaterials.8b00630
ACS Biomater. Sci. Eng. 2018, 4, 3347−3355

(7) O'Neill, R.; McCarthy, H. O.; Montufar, E. B.; Ginebra, M. P.; Wilson, D. I.; Lennon, A.; Dunne, N. Critical review: Injectability of calcium phosphate pastes and cements. *Acta Biomater.* **2017**, *50*, 1−19.
(8) Miyazaki, M.; Tsumura, H.; Wang, J. C.; Alanay, A. An update on bone substitutes for spinal fusion. *Eur. Spine J.* **2009**, *18*, 783−799.
(9) Acharya, N. K.; Kumar, R. J.; Varma, H. K.; Menon, V. K. Hydroxyapatite- bioactive glass ceramic composite as stand alone graft substitute for posterolateral fusion of lumber spine: a prospective, matched, and controlled study. *J. Spine Disord. Tech* **2008**, *21*, 106−111.
(10) Yamasaki, H.; Sakai, H. Osteogenic response to porous hydroxyapatite ceramics under the skin of dogs. *Biomaterials* **1992**, *13*, 308−312.
(11) Ripamonti, U. Bone induction in nonhuman primates. An experimental study on the baboon. *Clin. Orthop. Relat. Res.* **1991**, *269*, 284−294.
(12) Zhang, X.; Zhou, P.; Zhang, J.; Chen, W.; Wu, C. A study of porous block of HA ceramics and its osteogenesis. In *Bioceramics and the Human Body*; Ravaglioli, A, Krajewski, A, Eds.; Elsevier Science: Amsterdam, 1991; pp 408−415.
(13) Habibovic, P.; Yuan, H.; van der Valk, C. M.; Meijer, G.; van Blitterswijk, C. A.; de Groot, K. 3D microenvironment as essential element for osteoinduction by biomaterials. *Biomaterials* **2005**, *26*, 3565−3575.
(14) Kurashina, K.; Kurita, H.; Wu, Q.; Ohtsuka, A.; Kobayashi, H. Ectopic osteogenesis with biphasic ceramics of hydroxyapatite and tricalcium phosphate in rabbits. *Biomaterials* **2002**, *23*, 407−412.
(15) Yuan, H.; Kurashina, K.; de Bruijn, J. D.; Li, Y.; de Groot, K.; Zhang, X. A preliminary study on osteoinduction of two kinds of calcium phosphate ceramics. *Biomaterials* **1999**, *20*, 1799−1806.
(16) Chan, O.; Coathup, M. J.; Nesbitt, A.; Ho, C. Y.; Hing, K. A.; Buckland, T.; Campion, C.; Blunn, G. W. The effects of microporosity on osteoinduction of calcium phosphate bone graft substitute biomaterials. *Acta Biomater.* **2012**, *8*, 2788−2794.
(17) Davison, N. L.; Luo, X.; Schoenmaker, T.; Everts, V.; Yuan, H.; Barrère-de Groot, F.; de Bruijn, J. D. Submicron scale surface architecture of tricalcium phosphate directs osteogenesis in vitro and in vivo. *Eur. Cell Mater.* **2014**, *27*, 281−297.
(18) Zhang, J.; Luo, X.; Barbieri, D.; Barradas, A. M.; de Bruijn, J. D.; van Blitterswijk, C. A.; Yuan, H. The size of surface microstructures as an osteogenic factor in calcium phosphate ceramics. *Acta Biomater.* **2014**, *10*, 3254−3263.
(19) Duan, R.; Barbieri, D.; Luo, X.; Weng, J.; Bao, C.; de Bruijn, J. D.; Yuan, H. Variation of bone forming ability with the physicochemical properties of calcium phosphate bone substitutes. *Biomater. Sci.* **2018**, *6*, 136−145.
(20) Yang, Z.; Yuan, H.; Tong, W.; Zou, P.; Chen, W.; Zhang, X. Osteogenesis in extraskeletally implanted porous calcium phosphate ceramics: variability among different kinds of animals. *Biomaterials* **1996**, *17*, 2131−2137.
(21) Davison, N. L.; Gamblin, A. L.; Layrolle, P.; Yuan, H.; de Bruijn, J. D.; Barrère-de Groot, F. Liposomal clodronate inhibition of osteoclastgenesis and osteoinduction by submicrostructured β-tricalcium phosphate. *Biomaterials* **2014**, *35*, 5088−5097.
(22) Habibovic, P.; Yuan, H.; van den Doel, M.; Sees, T. M.; van Blitterswijk, C. A.; de Groot, K. Relevance of osteoinductive biomaterials in critical-sized orthotopic defect. *J. Orthop. Res.* **2006**, *24*, 867−876.
(23) Duan, R.; Barbieri, D.; Luo, X.; Weng, J.; de Bruijn, J. D.; Yuan, H. Submicron-surface structured tricalcium phosphate ceramics enhances the bone regeneration in canine spine environment. *J. Orthop. Res.* **2016**, *34*, 1865−1873.
(24) Yuan, H.; Fernandes, H.; Habibovic, P.; de Boer, J.; Barradas, A. M.; de Ruiter, A.; Walsh, W. R.; van Blitterswijk, C. A.; de Bruijn, J. D. Osteoinductive ceramics as a synthetic alternative to autologous bone grafting. *Proc. Natl. Acad. Sci. U. S. A.* **2010**, *107*, 13614−13619.
(25) Peters, F.; Reif, D. Functional materials for bone regeneration from beta-tricalcium phosphate. *Materialwiss. Werkstofftech.* **2004**, *35*, 203−207.
(26) Knabe, C.; Ducheyne, P. Cellular response to bioactive ceramics. In *Bioceramics and their Clinical Applications*; Kokutbo, T, Ed.; Woodhead Publishing Limited: Cambridge, U.K., 2008; pp 133−164.
(27) Guillaume, B. Filling bone defects with β-TCP in maxillofacial surgery: A review. *Morphologie* **2017**, *101*, 113−119.
(28) Tanaka, T.; Komaki, H.; Chazono, M.; Kitasato, S.; Kakuta, A.; Akiyama, S.; Marumo, K. Basic research and clinical application of beta-tricalcium phosphate (β-TCP). *Morphologie* **2017**, *101*, 164−172.
(29) Zheng, H.; Bai, Y.; Shih, M. S.; Hoffmann, C.; Peters, F.; Waldner, C.; Hübner, W. D. Effect of a b-TCP collagen composite bone substitute on healing of drilled bone voids in the distal femoral condyle of rabbits. *J. Biomed. Mater. Res., Part B* **2014**, *102*, 376−383.
(30) Zhang, Y.; Cui, X.; Zhao, S.; Wang, H.; Rahaman, M. N.; Liu, Z.; Huang, W.; Zhang, C. Evaluation of injectable strontium-containing borate bioactive glass cement with enhanced osteogenic capacity in a critical-sized rabbit femoral condyle defect model. *ACS Appl. Mater. Interfaces* **2015**, *7*, 2393−2403.
(31) Dupont, S.; Morsut, L.; Aragona, M.; Enzo, E.; Giulitti, S.; Cordenonsi, M.; Zanconato, F.; Le Digabel, J.; Forcato, M.; Bicciato, S.; Elvassore, N.; Piccolo, S. Role of YAP/TAZ in mechanotransduction. *Nature* **2011**, *474*, 179−183.
(32) Gattazzo, F.; Urciuolo, A.; Bonaldo, P. Extracellular matrix: a dynamic microenvironment for stem cell niche. *Biochim. Biophys. Acta, Gen. Subj.* **2014**, *1840*, 2506−2519.
(33) McNamara, L. E.; McMurray, R. J.; Biggs, M. J.; Kantawong, F.; Oreffo, R. O.; Dalby, M. J. Nanotopographical control of stem cell differentiation. *J. Tissue Eng.* **2010**, *18*, 120623.
(34) Kondo, N.; Ogose, A.; Tokunaga, K.; Umezu, H.; Arai, K.; Kudo, N.; Hoshino, M.; Inoue, H.; Irie, H.; Kuroda, K.; Mera, H.; Endo, N. Osteoinduction with highly purified beta-tricalcium phosphate in dog dorsal muscles and the proliferation of osteoclasts before heterotopic bone formation. *Biomaterials* **2006**, *27*, 4419−4427.
(35) Mitragotri, S.; Lahann, J. Physical approaches to biomaterial design. *Nat. Mater.* **2009**, *8*, 15−23.
(36) Steinberg, T.; Schulz, S.; Spatz, J. P.; Grabe, N.; Mussig, E.; Kohl, A.; Komposch, G.; Tomakidi, P. Early keratinocyte differentiation on micropillar interfaces. *Nano Lett.* **2007**, *7*, 287−294.
(37) Verma, A.; Uzun, O.; Hu, Y.; Hu, Y.; Han, H. S.; Watson, N.; Chen, S.; Irvine, D. J.; Stellacci, F. Surface-structure-regulated cell-membrane penetration by monolayer-protected nanoparticles. *Nat. Mater.* **2008**, *7*, 588−595.
(38) Fu, J.; Wang, Y. K.; Yang, M. T.; Desai, R. A.; Yu, X.; Liu, Z.; Chen, C. S. Mechanical regulation of cell function with geometrically modulated elastromeric substrates. *Nat. Methods* **2010**, *7*, 733−736.
(39) Abagnale, G.; Steger, M.; Nguyen, V. H.; Hersch, N.; Sechi, A.; Joussen, S.; Denecke, B.; Merkel, R.; Hoffmann, B.; Dreser, A.; Schnakenberg, U.; Gillner, A.; Wagner, W. Surface topography enhances differentiation of mesenchymal stem cells towards osteogenic and adipogenic lineages. *Biomaterials* **2015**, *61*, 316−326.
(40) Choi, C. H.; Hagvall, S. H.; Wu, B. M.; Dunn, JC. Y.; Beygui, R. E.; Kim, C. J. Cell interaction with three-dimensional sharp-tip nanotopography. *Biomaterials* **2007**, *28*, 1672−1679.
(41) Kolind, K.; Kraft, D.; Bøggild, T.; Duch, M.; Lovmand, J.; Pedersen, F. S.; Bindslev, D. A.; Bünger, C. E.; Foss, M.; Besenbacher, F. Control of proliferation and osteogenic differentiation of human dental-pulp-derived stem cells by distinct surface structures. *Acta Biomater.* **2014**, *10*, 641−650.
(42) Ariizumi, T.; Ogose, A.; Kondo, N.; Kawashima, H.; Hotta, T.; Kudo, N.; Hoshino, M.; Inoue, H.; Irie, H.; Endo, N. The role of microstructure of highly purified beta-tricalcium phosphate for osteoinduction in canine dorsal muscles. *J. Biomater. Nanobiotechnol.* **2013**, *4*, 189−193.

DOI: 10.1021/acsbiomaterials.8b00630
ACS Biomater. Sci. Eng. 2018, 4, 3347−3355

(43) Webster, T. J.; Schadler, L. S.; Siegel, R. W.; Bizios, R. Mechanism of enhanced osteoblast adhesion on nanophase alumina involve vitronectin. *Tissue Eng.* **2001**, *7*, 291−301.
(44) Boix, T.; Gómez-Morales, J.; Torrent-Burgués, J.; Monfort, A.; Puigdomènech, P.; Rodríguez-Clemente, R. Adsorption of recombinant human bone morphogenetic protein rhBMP-2m onto hydroxyapatite. *J. Inorg. Biochem.* **2005**, *99*, 1043−1050.
(45) Nakamura, S.; Matsumoto, T.; Sasaki, J.; Egusa, H.; Lee, K. Y.; Nakano, T.; Sohmura, T.; Nakahira, A. Effect of calcium ion concentrations on osteogenic differentiation and hematopoietic stem cell niche-related protein expression in osteoblasts. *Tissue Eng., Part A* **2010**, *16*, 2467−2473.
(46) Barradas, A. M.; Fernandes, H. A.; Groen, N.; Chai, Y. C.; Schrooten, J.; van de Peppel, J.; van Leeuwen, J. P.; van Blitterswijk, C. A.; de Boer, J. A. calcium-induced signaling cascade leading to osteogenic differentiation of human bone marrow-derived mesenchymal stromal cells. *Biomaterials* **2012**, *33*, 3205−3215.
(47) Heymann, D.; Pradal, G.; Benahmed, M. Cellular mechanisms of calcium phosphate ceramic degradation. *Histol. Histopathol.* **1997**, *14*, 871−877.
(48) Yamada, S.; Heymann, D.; Bouler, J. M.; Daculsi, G. Osteoclastic resorption of calcium phosphate ceramics with different hydroxyapatite/beta-tricalcium phosphate ratios. *Biomaterials* **1997**, *18*, 1037−1041.
(49) Kondo, N.; Ogose, A.; Tokunaga, K.; Ito, T.; Arai, K.; Kudo, N.; Inoue, H.; Irie, H.; Endo, N. Bone formation and resorption of highly purified beta-tricalcium phosphate in the rat femoral condyle. *Biomaterials* **2005**, *26*, 5600−5608.
(50) Davison, N. L.; ten Harkel, B.; Schoenmaker, T.; Luo, X.; Yuan, H.; Everts, V.; Barrère-de Groot, F.; de Bruijn, J. D. Osteoclast resorption of beta-tricalcium phosphate controlled by surface architecture. *Biomaterials* **2014**, *35*, 7441−7451.

DOI: 10.1021/acsbiomaterials.8b00630
ACS Biomater. Sci. Eng. 2018, 4, 3347−3355